JOURNAL OF CHEMICAL INFORMATION AND MODELING

Article

pubs.acs.org/jcim

β-Amyloid and Neprilysin Computational Studies Identify Critical Residues Implicated in Binding Specificity

Darrick Pope, Jeffry D. Madura, and Michael Cascio*

Department of Chemistry and Biochemistry and Center for Computational Sciences, Duquesne University, 600 Forbes Avenue, 331 Mellon Hall, Pittsburgh, Pennsylvania 15282, United States

Supporting Information

ABSTRACT: The zinc metalloprotease neprilysin (NEP) promiscuously degrades small bioactive peptides. NEP is among a select group of metalloenzymes that degrade the amyloid beta-peptide (Aβ) in vivo and in situ. Since accumulation of neurotoxic Aβ aggregates in the brain appears to be a causative agent in the pathophysiology of Alzheimer's disease (AD), increased clearance of Aβ resulting from overexpression of NEP exhibits therapeutic potential for AD. However, higher NEP peptidase activity may be harmful without an increased specificity for Aβ over other competing substrates. Crystal structures of NEP−inhibitor complexes and their characterization have highlighted potential amino acid interactions involved in substrate binding and are used as templates to guide our methodology in docking Aβ in NEP. Results from protein−ligand docking calculations predict S2′ subsite residues Arg 102 and Arg 110 of NEP participate in specific interactions with Aβ. These interactions provide insight into developing NEP specificity for Aβ.

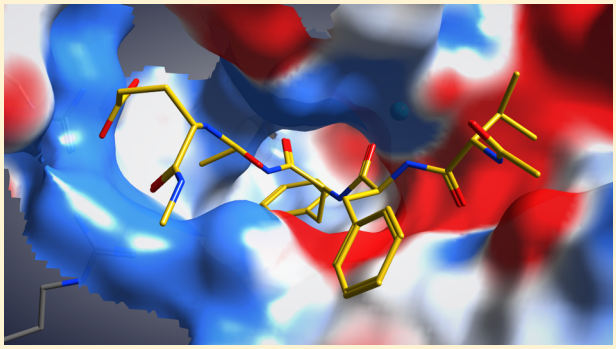

INTRODUCTION

Neprilysin (NEP, also known as enkephalinase or neutral endopeptidase, EC 3.4.24.11) is a type II integral membrane protein that belongs to the M13 subfamily of zinc-dependent metalloendopeptidases.[1] Among other activities, this family proteolyzes and terminates the signaling activities of small bioactive peptides, such as enkephalin, angiotensin, bradykinin, and atrial natriuretic peptides as well as Tachykinins.[2,3] NEP and other metalloendopeptidases (such as insulin-degrading enzyme, matrix metalloproteinase-9, and angiotensin converting enzyme) have been studied extensively for their role in degradation and clearance of the amyloid beta-peptide (Aβ).[4−6] Increasing interest in Aβ catabolism has correlated with more widespread acceptance of the amyloid cascade hypothesis, a two-decades old theory that proposes Aβ accumulation and deposition onto nerve cells is the "primary influence driving AD pathogenesis."[7] Researchers have hypothesized that the accumulation of Aβ observed in late-onset Alzheimer's disease (AD) is caused in part by the decline of Aβ clearance from neural pathways,[8,9] and recent studies point to the prefibrillar polypeptide oligomers of Aβ as the primary toxicological form.[10−16] Evidence linking Aβ accumulation and AD has prompted numerous studies of Aβ aggregation and catabolism, with many studies focused on the prevention of Aβ accumulation using Aβ-degrading peptidases (such as NEP) that reduce the amount of neural Aβ available for formation of oligomers, fibrils, and plaques.[17−23]

As a principal peptidase in the degradation of Aβ, NEP has been studied extensively in vitro and in vivo.[4,24−30] Transgene NEP expression decreased neuronal Aβ deposits and attenuated neurodegenerative processes in an AD mouse model.[31−33] Overexpression of soluble NEP in a number of other animal studies also resulted in significant decreases in levels of neural Aβ and improved cognitive performance.[34−37] Activity of NEP in human brain tissue was shown to increase with normal aging, but further elevated levels were detected in correlation with indicators of AD progression.[4] The wealth of evidence linking Aβ accumulation with NEP activity in disease models of AD suggests that this peptidase is a promising therapeutic agent for reducing Aβ load in AD.

While the proteolytic activity of NEP has been observed to significantly reduce Aβ peptide accumulation, other neuropeptide targets are also degraded by this fairly nonspecific enzyme.[2,3,38] Excessive amounts of NEP would most likely lead to dangerous imbalances of neuropeptides in signal pathways that control blood pressure, pain, and other crucial physiological processes. A solution to this potential issue may be the use of site-directed mutagenesis to engineer a form of NEP that favors degradation of Aβ over other substrates. This engineering approach has been used successfully on other promiscuous enzymes,[39] but a recent mutagenesis study of NEP did not observe any increased specificity for Aβ or other various substrates.[40] Engineering an NEP peptidase for AD therapy appears to be problematic without detailed knowledge of specific interactions involved in Aβ binding.

Received: January 9, 2014
Published: March 20, 2014

dx.doi.org/10.1021/ci500015m | J. Chem. Inf. Model. 2014, 54, 1157−1165

Current knowledge of the NEP binding pocket centers on the amino acid residues surrounding its zinc(II) ion (Zn^{2+}) cofactor. X-ray crystallographic studies of seven different inhibitor-bound NEP complexes indicate that the Zn^{2+} is coordinated to a bound ligand by two conserved, consensus sequences: ^{583}HExxH^{587} and ^{646}ExxxD^{650}.[41−46] In addition, E584 appears to be involved in a complex hydrogen (H) bonding network with N542 and A543 of a consensus NAFY motif as well as R717, H711, and other residues around the NEP binding pocket.[42] The crystal structures verified prior efforts to group NEP residues into binding subsites[47] and label them with Schechter and Berger notation,[48] which uses the letter S and a number to represent the relative position of pocket residues to ligand atoms that are labeled correspondingly using the letter P. The NEP residues Y545 and E584 of the S1 site interact with P1 atoms located on the amino terminal side of a substrate's carbonyl-amide scissile bond. Residues on the carboxy terminal side of the scissile bond contain P1′ atoms that interact with NEP residues of the S1′ site that includes N542, V580, and R717. The numbers for S and P sites on either side of the scissile bond increase by one for each subsequent substrate residue, such that P2′ atoms of a substrate interact with residues lining the S2′ in NEP (these include R102 or R110). Unfortunately, none of the NEP crystal structures have bound endogenous peptide substrates but, rather, are complexed with nonhydrolyzable competitive inhibitors that are not peptides. Similarities between the inhibitors and peptides do facilitate the conventional assignment of S and P sites,[41] which simplifies a comparative analysis with peptidic substrates. The major shortcoming of current NEP crystal structures is that the bound inhibitors are peptidomimetics that are much smaller than Aβ and many other polypeptide substrates of NEP, thus limiting observed binding interactions to a few S subsites near the scissile bond. We have previously reviewed how the crystal structures in combination with other NEP structural data may help identify common interactions with substrates and elucidate the relative specificity of NEP, as well as provide insights regarding its potential therapeutic utility.[49]

Building from experimental data on NEP structure, other groups have utilized computational chemistry to model common NEP binding interactions with various ligands.[50,51] Docking simulations with NEP inhibitors have identified binding interactions and free energies ($\Delta G°$) that are consistent with experimental data,[51] suggesting that the interactions stabilizing a ligand in the NEP pocket may be accurately modeled. In this study we have modeled the interactions of NEP with four inhibitors (Figure 1) and three sequences of Aβ using the Molecular Operating Environment program (MOE).[52] MOE is often used as a tool for structure-based drug design, as the MOE Dock module searches for favorable binding configurations (poses) between small- to medium-sized ligands and a semirigid target protein. Recently, docking of ligand−enzyme complexes with MOE Dock was tested with an ACS-Astex data set and demonstrated an 80% success rate in producing a top-ranked pose of ligand atoms within a root-mean-square deviation (RMSD) of 2 Å to the corresponding crystal structure.[53] We used MOE Dock to generate NEP−ligand binding poses and then relaxed the binding complexes with molecular dynamics (MD) simulations. In modeling NEP binding complexes with MOE MD, $\Delta G°$ values were estimated with generalized Born volume integral (GBVI) and Poisson−Boltzmann plus surface area (PBSA) scoring functions. GBVI and PBSA scoring functions have been thoroughly evaluated for their accuracy, precision, and stability in MD while becoming popular tools for estimating protein−ligand affinities.[54,55] The predictive capabilities of this study's methodology was evaluated by comparing our NEP−inhibitor models to known experimental structures and $\Delta G°$ data from identical and closely related inhibitors. Upon validation of the methodology with the inhibitors, modeling studies were subsequently conducted on the interactions of NEP with sequences of Aβ to identify subsite amino acids that interact with Aβ and suggest mutations of NEP that may increase selectivity for this substrate.

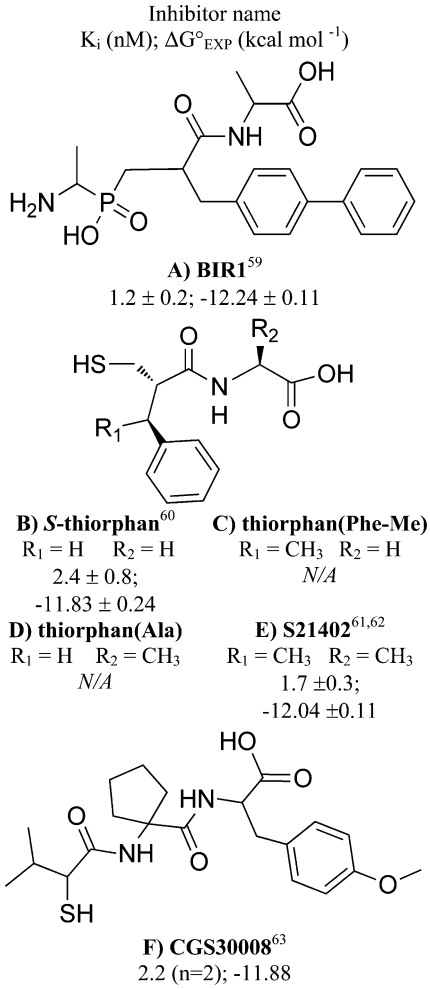

Figure 1. Line structures, K_i, and calculated experimental binding free energies ($\Delta G°_{EXP}$) of NEP inhibitors.

COMPUTATIONAL METHODS

Structure Preparation. Interactions of NEP binding with various ligands were simulated using MOE.[52] Coordinates of the non-H atoms in the NEP crystal structure were taken from the protein database file (PDB) 1r1h of NEP with bound inhibitor BIR1.[41] The Structure Preparation module of MOE added the missing H atoms and addressed basic structural issues. Ligands were assembled in MOE using the Molecule and Protein Builder features, with an NMR structure as a template for Aβ (PDB: 1y1t).[56] The empty binding pocket of the NEP structure was relaxed with Energy Minimization, a molecular mechanics application of MOE. Minimization was terminated when the root-mean-square (RMS) gradient of the potential

dx.doi.org/10.1021/ci500015m | J. Chem. Inf. Model. 2014, 54, 1157−1165

energy fell below 0.1, according to the AMBER-based PFrosst force field.[57] Prior to running Dock with the prepared NEP pocket, a series of conformations for each isolated ligand were generated using the MOE Conformational Search feature.

Docking. The conformations of a ligand (Figure 1) and the prepared NEP structure were loaded into MOE Dock to generate an initial set of docked poses. Poses of the smaller inhibitors S21402 and *S*-thiorphan were placed in the NEP pocket using the Triangle Matcher method, while poses of the other inhibitors and *Aβ* were placed using Proxy Triangle. Conformations in this second method are presuperposed prior to placement and the internal scoring of the poses uses structural representations instead of all the atoms of the ligand. Following placement, ligand poses were rescored with functions that estimated the $\Delta G^{\circ}_{\text{binding}}$ in kilocalories per mole. After rescoring with the London ΔG° function, the poses were ranked and the top one hundred poses with the lowest scores were retained for the final stages of Dock. Each NEP−inhibitor pose was energy minimized using Force Field Refinement, a molecular mechanics feature in Dock. A final dock score for the 100 ligand poses was calculated with the force field-based GBVI/WSA (weighted surface area) ΔG° scoring function.

Molecular Dynamics. Top ranking poses of each NEP−ligand complex were visually inspected before use as starting structures for MOE MD. The protonation states of certain pocket residues, most often H711 and E584, were assigned to be consistent with crystal structure nitrogen and oxygen atoms at proximities that were indicative of hydrogen bonding interactions. In preparation for MOE MD, the backbone and side-chain atoms outside the NEP pocket were put on a 1 Å tether with a weight of 10 (~2.7 kcal mol^{-1} resistance at 2 Å), while pocket side-chain or ligand atoms were tethered only to preserve interactions during solvation, energy minimization, and equilibration of the structure. The binding pocket was solvated by addition of explicit water molecules within a 10 Å walled ellipse (weight = 20) around the pocket. Explicit waters within 10 Å of the pocket were tagged for the wall limit, while waters outside 10 Å were assigned a 1 Å tether of 300 (~81 kcal mol^{-1} resistance at 2 Å). The solvated NEP complex was then energy minimized to an RMS gradient of 0.01 with the PFrosst force field as implemented in MOE. Between minimization steps, the charges of the ligand atoms were reassigned according to the AM1-BCC charge model.[58] Charges and tethers of NEP complexes were preserved during the equilibrium and production phases of Nosé−Poincaré−Anderson MD. Each NEP complex was subjected to an initial equilibrium simulation ranging from 250 to 500 ps that allowed for thorough solvation of the NEP complex. After a NEP system was re-evaluated by inspection, the ligand−NEP binding was modeled in an MD simulation with a 100 or 150 ps equilibrium phase followed by a 500 ps production phase. During both phases, atomic forces and trajectories of the NEP system were calculated at each time step of 0.001 ps. Calculations of these properties were recorded in a trajectory file at time periods of 0.5 ps throughout the simulation. Molecular mechanics GBVI and PBSA scores ($\Delta G^{\circ}_{\text{GBVI}}$ and $\Delta G^{\circ}_{\text{PBSA}}$, respectively) were calculated for sample trajectories and averaged over multiple independent MD simulations of each NEP complex.

RESULTS

Modeling of Inhibitors in NEP. Computational simulations of NEP with known inhibitors BIR1, *S*-thiorphan, S21402, or CGS30008 (Figure 1), were conducted to evaluate the predictive capabilities of our docking and MD methodologies using either a GBVI or PBSA-based scoring function.

Initially, the docking methodology generated six to ten thousand poses of each inhibitor in the binding pocket of NEP by multiple rounds of MOE Dock. When a round of docking produced highly ranked inhibitor poses that shared the common interactions and geometries of a single NEP binding mode, a representative binding mode pose was selected as the basis for modeling in MOE MD. Poses in MD were monitored for the stability of the NEP binding mode by calculations of inhibitor atom RMSD, which were then plotted for analysis (see Supporting Information Figures S1−S4). To assess the validity of each modeled NEP−inhibitor complex, the experimentally determined Zn^{2+} coordination distance and binding ΔG° value of each inhibitor was compared to the estimated values for the corresponding NEP−inhibitor model, using the average Zn^{2+} distance during MD and binding ΔG° scores from calculations with GBVI (reported as $\Delta G^{\circ}_{\text{GBVI}}$) and PBSA ($\Delta G^{\circ}_{\text{PBSA}}$). Computed ΔG° scores were averaged over the production phases of three separate MD simulations, each starting with a different pose of the corresponding NEP−inhibitor binding mode.

Docking of BIR1 and *S*-thiorphan inhibitors with NEP resulted in model complexes that compared favorably to corresponding crystal structures[41,44,64] with respect to the orientation of inhibitor atoms with Zn^{2+} and the S subsites of NEP (Figure 2A and B). The BIR1 model identified by docking was similarly oriented within the NEP S1, S1′, and S2′ subsites (Figure 2A) as the BIR1 structure in the 1r1h crystal structure,[41] including H-bonding distances with N542, A543, E584, H711, and R717. The only significant deviation in the atomic distances between the BIR1 model and the 1r1h structure is a smaller distance between NEP H711 and the P1′ carbonyl group of an average BIR1 pose (2.27 versus 3.01 Å from the 1r1h structure). Over the 500 ps duration of the three BIR1 MD simulations, the average model distances of the Zn^{2+} from atoms in the NEP residues H583 (2.14 Å), H587 (1.94 Å), E646 (1.73 Å), and a BIR1 phosphinic oxygen (1.75 Å) were relatively comparable to the distances of the crystal structure atoms (2.04, 2.12, 1.98, and 1.94 Å respectively).[41] The NEP model with *S*-thiorphan (Figure 2B) also compared favorably to previous NEP models based on a crystal structure for the NEP homologue Thermolysin (PDB: 1zdp).[44,64] The bacterial enzyme Thermolysin contains analogous pocket structures that have been used by other groups to model NEP binding interactions with thiorphan.[44,60,65,66] The *S*-thiorphan model and crystal structure both indicate a dual hydrogen bonding interaction with N542 in the NEP S2′ site, the inhibitor phenyl group near S1′ residues V580, W693, and R717 as well as sulfhydryl coordination with Zn^{2+} and H711. Parallels with experimental observations were preserved in MD simulations, including the average model distances of the Zn^{2+} to NEP H583 (2.18 Å), H587 (2.20 Å), E646 (1.80 Å), and the ligand sulfur atom (2.04 Å) compared to crystal structure distances (1.88, 1.94, 1.87, and 2.12 Å, respectively).[44,64]

A model of S21402 bound to NEP (Figure 2B) was constructed from critical evaluation of the top 50 ranked poses that resulted after two rounds of docking. Most top ranked poses of S21402 shared a dual binding interaction with NEP N542 similar to that of the *S*-thiorphan model and crystal structure, but an alternative set of S21402 poses with the terminal carboxyl group binding instead to NEP R102 also

dx.doi.org/10.1021/ci500015m | J. Chem. Inf. Model. 2014, 54, 1157−1165

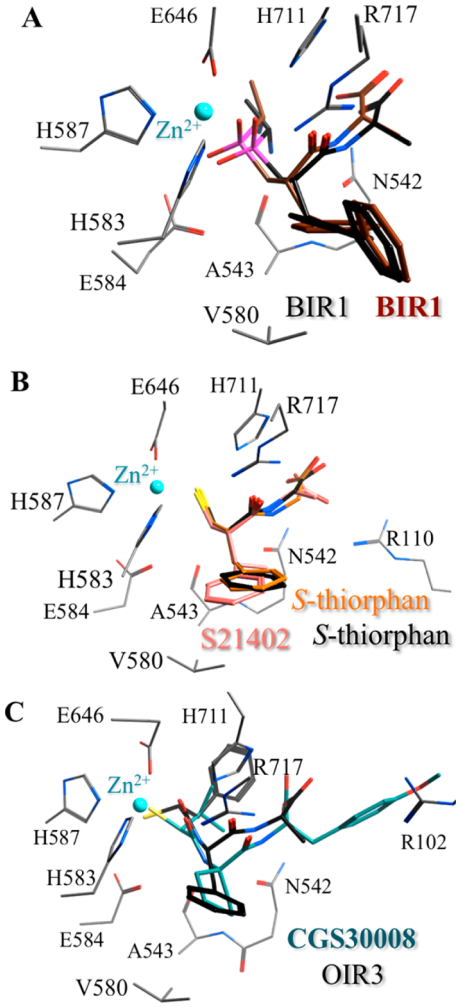

Figure 2. Representative poses of NEP-bound inhibitor models superimposed with similar inhibitors from crystal structures (in black): (A) BIR1 (PDB: 1r1h)[41] model in brown, (B) *S*-thiorphan (PDB: 1zdp)[44,64] model in orange and S21402 in salmon, and (C) CGS30008 in cyan (OIR3 PDB: 1r1j).[41] The coordinating Zn^{2+} is bright teal, and key pocket residues are gray (other residues omitted for clarity).

ranked highly in docking results. To test if the methyl groups unique to S21402 favored one of the binding modes, we performed docking studies with two new structures, thiorphan-(Phe-Me) and thiorphan(Ala) (Figure 1C and D). From docking of the test structures, thiorphan(Ala) favors R102 binding in the simulations while thiorphan(Phe-Me) favors binding with N542 (unpublished observation). Notably, the top ranked N542-binding poses of thiorphan(Phe-Me) and S21402 positioned the sulfur atom within binding distance of the NEP R717 side-chain. The R717 interaction with the sulfhydryl group of S21402 is unique to our NEP model, which also includes the carboxyl group oriented near NEP residues N542 and R110 (Figure 2B) similar to the *S*-thiorphan crystal structure model[44,64] and a model of S21402 in NEP from an independent study.[51]

The highest-ranking poses of CGS30008 (Figure 1F) in NEP resulted from docking of an inhibitor structure with a deprotonated sulfhydryl group. Deprotonation of the sulfhydryl was only predicted for poses of CGS30008 closely coordinated to the Zn^{2+} via the inhibitor sulfur atom, which is consistent with NEP crystal structures of two analogous inhibitors.[41]

In further agreement with the crystal structures,[41] the mercaptoacyl group of our CGS30008 model forms a bidentate interaction with the Zn^{2+} in an approximately trigonal bipyramidal geometry with the coordinating residues of NEP (Figure 2C). Atoms of the CGS30008 mercaptoacyl remained closely coordinated to the Zn^{2+} during MD, with average distances of 1.92 and 2.59 Å for the sulfur and oxygen, respectively. Overall, the position of CGS30008 in our model coordinated the inhibitor isopropyl group in the NEP S1 site, the cyclopentyl in the S1′, the carboxyl group with N542, and the methoxyphenyl in the S2′.

ΔG° Correlation Analysis. The validity of our NEP−inhibitor models was further evaluated by examining the correlation between model scoring estimates of binding ΔG° (ΔG°_{GBVI} and ΔG°_{PBSA}) and experimentally measured values from NEP inhibition studies (ΔG°_{EXP}; see Figure 1 and references therein). The ΔG°_{EXP} of the NEP inhibitors were proportionally less negative than the ΔG°_{GBVI} and ΔG°_{PBSA} scores for the NEP−inhibitor models. Inspection of calculated values for the PBSA and GBVI scoring equations has indicated that the polar solvation energy components of the $\Delta G^\circ_{GBVI}/\Delta G^\circ_{PBSA}$ calculations was uniformly underestimated. We hypothesize that this resulted in the over 300 kcal/mol difference between the $\Delta G^\circ_{GBVI}/\Delta G^\circ_{PBSA}$ scoring estimates and ΔG°_{EXP}. To account for the disparity in scale between the $\Delta G^\circ_{GBVI}/\Delta G^\circ_{PBSA}$ scores and the ΔG°_{EXP} values, we compared the relative differences in binding ΔG° scores for the NEP models to the experimental values for the NEP inhibitors.

Graphical analyses of the correlations between model and experimental ΔG° values were conducted by plotting the mean and standard deviation of inhibitor ΔG°_{GBVI} and ΔG°_{PBSA} scores as the dependent variable to independent ΔG°_{EXP} values (Figure 3A and B). A linear fit and Pearson's correlation coefficient (R) were calculated for each ΔG° correlation plot using the mean values of the reported ΔG°_{EXP}. The R^2 values of 0.76 for ΔG°_{GBVI} (Figure 3A) and 0.92 for ΔG°_{PBSA} (Figure 3B) display a moderate to strong correlation with ΔG°_{EXP}, indicating that our GBVI and PBSA scoring methods reproduced the observed trend in NEP−inhibitor binding affinity. In conjunction with comparisons to structural data, the linear correlation of model ΔG° scores to ΔG°_{EXP} validates that our computational methodology was sufficient to sensitively differentiate NEP−inhibitor binding interactions and predict the relative free energies of those interactions.

Overall, the models of all NEP−inhibitor complexes were consistent with experimental data, including GBVI and PBSA estimates of ΔG° that correlated to ΔG°_{EXP}. Agreement of our proposed NEP−inhibitor models with experimental studies represents the principal validation of our modeling methodology, which was then used to subsequently investigate the interaction of NEP with Aβ.

Modeling of Aβ in NEP. As described earlier, overexpression of NEP can limit Aβ accumulation associated with AD.[31−37] The Aβ peptide seems to be an unusually large substrate for NEP, as most of the peptidase targets are less than 3 kDa in size.[2,3] The NEP structure surrounding the binding pocket appears to favor relatively small peptides, particularly because of a second protein domain (or domain 2) adjacent to the NEP pocket.[41−46] Domain 2 is observed in mammalian peptidases (but not bacterial) of the NEP family, and substrates are believed to reach the NEP pocket via domain 2 by passing through a small, circular opening enclosed by charged residues that would act as a molecular sieve.[42] The absence of a domain

dx.doi.org/10.1021/ci500015m | J. Chem. Inf. Model. 2014, 54, 1157−1165

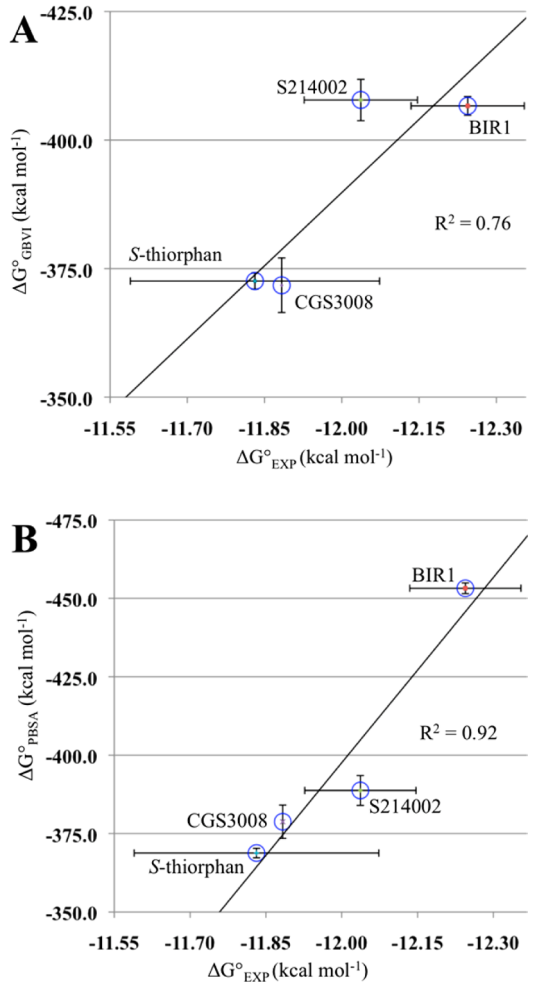

Figure 3. Correlation plot of inhibitor (A) ΔG°_{GBVI} scores or (B) ΔG°_{PBSA} scores with ΔG°_{EXP} as the independent variable. In each panel, the R^2 value is provided for the linear fit between the mean ΔG°_{EXP} and ΔG°_{PBSA} or ΔG°_{GBVI} scores of each inhibitor.

2 from bacterial structures has led to the hypothesis that this sieve in NEP causes the relative selectivity for smaller substrates. Given that NEP domain 2 limits the size of and access to the binding pocket, stretches of five amino acid residues in the Aβ sequence were considered to be sufficient in modeling the interaction of Aβ with NEP. The Aβ models in this study were based on distinct residue sequences, VFFAE ($A\beta_{18-22}$) and SGYEV ($A\beta_{8-12}$), that incorporate two consensus scissile bond sites cleaved by NEP (F^{19}–F^{20} and G^{9}–Y^{10}, respectively; Figure 4), as indicated by LC-MS studies.[40,67,68] In addition, the point mutation A21G (or Flemish) in Aβ has been linked to a hereditary disease with AD-like symptoms.[69] The A21G substitution in Aβ results in a 300–350% decreased rate of peptide degradation by NEP.[70] Thus, the interaction of NEP with the Flemish mutation, VFFGE, was modeled for comparison with NEP–$A\beta_{18-22}$, particularly for an anticipated difference in the ΔG°_{GBVI} and ΔG°_{PBSA} scores of the respective models that may reflect a lower binding affinity and, hence, a reduced efficacy of clearance for the A21G mutation. Likewise, we hypothesized that the model of $A\beta_{8-12}$ in NEP will have reduced affinity for NEP (increased relative calculated ΔG° scores), in agreement with observations of NEP hydrolysis of Aβ at G^{9}–Y^{10} proceeding more slowly or even secondarily to F^{19}–F^{20}.[40,67,68] Modeling of NEP interactions with the three Aβ sequences began with construction of Aβ sequence structures based on the NMR structure of Aβ (PDB: 1y1t).[56] As a result, the preliminary constructs of Aβ sequences incorporated α-helical geometry similar to the 1y1t NMR structure. The Aβ sequence constructs were then docked and modeled in NEP using the same MOE methodology validated with the NEP inhibitors.

Models of $A\beta_{18-22}$ and $A\beta_{18-22}$(A21G) with NEP. In three rounds of docking $A\beta_{18-22}$, the poses with V^{18} at the P1 position to E^{22} at the P4′ consistently outranked any other poses with (or even without) the scissile carbonyl coordinated to the Zn^{2+} in NEP. Analysis of the NEP-bound $A\beta_{18-22}$ poses indicated that the (P2) V^{18}–E^{22} (P3′) orientation favored bonding interactions between the side-chain carboxyl group of E^{22} and NEP R102/R110 (Figure 5). One of the NEP crystal

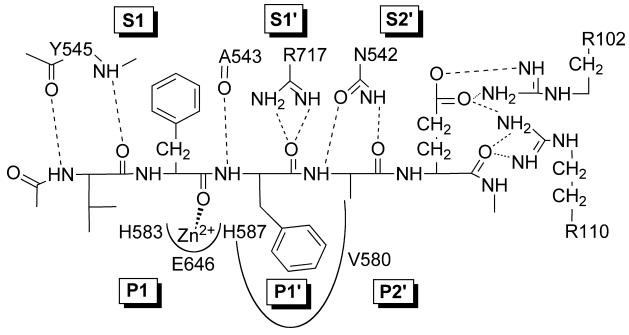

Figure 5. Line drawing of the NEP model bound to the $A\beta_{18-22}$ sequence. The substrate and NEP subsites are labeled with P and S designations, respectively. Dashed lines show key binding interactions.

structures contains a bound inhibitor that also interacts with both R102 and R110 (PDB: 2yb9).[43] Other experimentally observed residue interactions predicted by the top ranked poses included F^{20} of Aβ within the NEP S1′ site and hydrogen

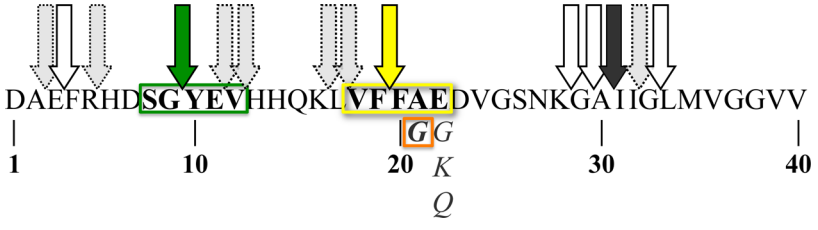

Figure 4. $A\beta_{40}$ sequence with disease-related amino acid substitutions represented by italicized letters below the sequence (presentation inspired by the work of Hersh and Rodgers).[20,71] The general sequences modeled in this study are shown by the box outlines (the third sequence included the A21G substitution). Arrows indicate the NEP cleavage sites identified by LC-MS studies of Aβ peptide degradation:[40,67,68] solid colored arrows are for the consensus cleavage sites, and dotted–shaded or open arrows are for sites identified in one or two of the studies, respectively.

dx.doi.org/10.1021/ci500015m | J. Chem. Inf. Model. 2014, 54, 1157–1165

Table 1. Residue Interactions and Binding Free Energies Predicted for the Aβ Sequence Models

Aβ sequence model	model binding ΔG° estimates[a] (kcal mol^{-1}) and interactions		
	ΔG°_{GBVI}	ΔG°_{PBSA}	NEP residue interactions[b]
$A\beta_{18-22}$	−191.0 ± 3.8	−232.0 ± 3.5	R102, **R110**, **N542**, **A543**, F544, **Y545**, F563, V580, H583, W693, H711, **R717**
$A\beta_{18-22}$(A21G)	−177.6 ± 3.5	−217.4 ± 3.2	R102, **R110**, **N542**, **A543**, F544, **Y545**, F563, V580, H583, W693, H711, **R717**
$A\beta_{8-12}$	−163.6 ± 1.2	−205.7 ± 1.7	R102, R110, **N542**, **A543**, F544, **Y545**, V580, W693, H711, **R717**

[a]Averaged scores from 150 ps periods of molecular dynamics simulations ($n \geq 4$) were obtained using the molecular mechanics GBVI and PBSA ΔG° scoring functions. [b]Residues involved in salt bridge interactions are underlined, those forming hydrogen bonds are in bold, and those involved in van der Waals interactions are in plain font.

bonding with the R717 side-chain as well as three residues of the NEP NAFY motif. Multiple MD simulations with similar poses of $A\beta_{18-22}$ identified a highly stable model complex that included all of these NEP residue interactions (Table 1).

We postulate that a decreased rate of NEP degradation for the A21G form of Aβ results from a similar binding mode for the mutant form (as compared to its wild type counterpart) with decreased NEP binding affinity and is not a result of an alternative binding mode. The similarity in binding modes for both forms is supported by direct comparison of models of NEP binding to $A\beta_{18-22}$ with $A\beta_{18-22}$(A21G). Docking of $A\beta_{18-22}$(A21G) followed the procedure described above for $A\beta_{18-22}$ and produced top ranked poses of $A\beta_{18-22}$(A21G) with similar orientation and residue interactions as $A\beta_{18-22}$ (Table 1). When superimposed with one another, representative poses of the two Aβ sequence models had an RMSD of less than 0.25 Å. The only significant difference observed for the modeling of $A\beta_{18-22}$(A21G) was in the ΔG° scores. The ΔG°_{GBVI} of −177.6 ± 3.5 and ΔG°_{PBSA} of −217.3 ± 3.2 were significantly less negative than the corresponding values for $A\beta_{18-22}$ model (−191.0 ± 3.8 and −232.0 ± 3.5; Table 1), which is consistent with the observed slower NEP-dependent rate of Aβ degradation for the A21G mutation[70] being due to reduced relative binding affinity toward this substrate.

Model of $A\beta_{8-12}$ with NEP. Similar to $A\beta_{18-22}$, the $A\beta_{8-12}$ sequence contains an isolated consensus target site for NEP-mediated hydrolysis, which is the scissile bond of G^9–Y^{10} (Figure 4). However, NEP hydrolysis within $A\beta_{18-22}$ has been observed to precede that of $A\beta_{8-12}$, suggesting that NEP may have a weaker binding affinity for $A\beta_{8-12}$.[40,67,68] In agreement with this theory, the model of $A\beta_{8-12}$ in NEP predicted reduced relative affinity in the GBVI and PBSA estimates of ΔG° (Table 1). The $A\beta_{8-12}$ model was derived from a collection of poses obtained by docking with NEP structures from the inhibitor and $A\beta_{18-22}$ models. After three rounds of docking $A\beta_{8-12}$, preliminary MD with a few distinct poses revealed a single, stable model of binding that oriented the S^8 to V^{12} sequence from the S1 to S2′ of NEP (Figure 6). Of note, the average distance between the G^9–Y^{10} scissile carbonyl and the Zn^{2+} was greater in both MD simulations of $A\beta_{8-12}$ (at 1.950 and 1.972 Å, respectively) than for any simulation with the $A\beta_{18-22}$ sequences.

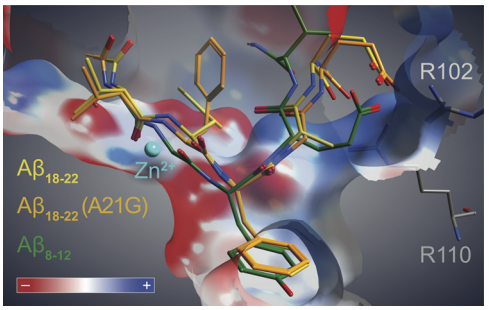

Figure 6. Representative poses of the NEP-bound models with $A\beta_{18-22}$ in yellow, $A\beta_{18-22}$(A21G) in orange, and $A\beta_{8-12}$ in green. The electrostatic surface of the NEP binding pocket is shown, with regions of negative (red) and positive (blue) charge. The coordinating Zn^{2+} is colored in bright teal, and R102/R110 pocket residues are in gray (other residues omitted for clarity). The $A\beta_{18-22}$ pose had an averaged backbone atom RMSD of 0.24 Å with $A\beta_{18-22}$(A21G) and 1.77 Å with $A\beta_{8-12}$.

DISCUSSION

The results of our computational study demonstrate a potential advancement in understanding substrate binding to NEP. Continued evaluation of the methodology with NEP inhibitors may further demonstrate the predictive power of the NEP modeling methodology. For example, we found that the models of structurally similar *S*-thiorphan and S21402 inhibitors (Figure 2B) have considerably higher ΔG°_{GBVI} than ΔG°_{PBSA} values, which lead to over- or underestimates of the linear fit in the correlation plots of those respective scores (Figure 3A and B). When the mean of the ΔG°_{GBVI} and ΔG°_{PBSA} scores ($\Delta G^\circ_{GBVI-PBSA}$) from each of the inhibitors was plotted against the mean ΔG°_{EXP}, a higher correlation was observed with an R^2 of 0.99 (Supporting Information Figure S5). The strong correlation of our models to experimental data shows the capability of the methodology to predict the relative strength of NEP–inhibitor binding interactions.

In regards to better understanding the binding of NEP with peptides (rather than peptidomimetics), our models of NEP with docked Aβ substrates highlight similar binding modes for multiple substrates involving interactions with the peptide backbone of the substrate. The small (<2 Å) backbone RMSD of the superposed Aβ sequences coincides with Aβ backbone atoms forming many of the binding interactions with NEP pocket residues, consistent with the promiscuity of NEP selectivity. Binding interactions between NEP and the Aβ backbone are very similar to NEP interactions observed in structural studies with various peptidomimetic inhibitors, as specific residues in the S1, S1′, and S2′ of NEP are positioned to similarly bind with both inhibitors and peptide targets. Of note, a majority of NEP peptide substrates contain a large, hydrophobic group at the P1′ or P2′ position that appears to be accommodated by the S1′ or S2′ subsites of NEP.[41] The models of Aβ are aligned so that the phenyl containing side-chains of the peptide are positioned in the large, hydrophobic S1′ site of NEP. Overall, the models of NEP and Aβ highlight pocket residues and subsites that appear to underlie the peptidase's limited substrate specificity.

While many of the observed substrate binding interactions involve peptide backbone interactions in the binding pocket and thus are sequence independent, predicted residue-specific

interactions unique to our models of Aβ in NEP may be important in directing NEP binding preferences. In these models, each Aβ sequence forms binding interactions with R102 and R110 in the S2′ site of NEP (Figure 6). A binding role for R102 was also implicated by experimental substitutions of K, G, Q, and E for R102, which resulted in lower NEP binding affinity for certain peptide inhibitors (including Phe-Ala).[72] Similar experimental studies involving substitutions to R102/R110 would be useful to refine and verify the model of NEP−Aβ obtained by our methodology. In addition, site-directed mutagenesis studies of S2′ residues can then critically test for enhanced specificity of NEP to target substrates. Random mutation of promiscuous proteases has demonstrated that substitution of residues on the perimeter of the active sites can alter or tune the binding specificity.[39] With validated NEP-bound substrate models as a blueprint, the tuning the proteolytic specificity of NEP could result in mutated forms of NEP that offer novel therapeutic potential.

The most relevant disease-related application of the NEP−Aβ models is in development of a potential therapeutic for AD. Transgene expression or injections of soluble NEP have been used to reduce the accumulation of Aβ and other symptoms of AD in animal models. Hereditary, AD-like diseases in humans are associated with five point mutations to Aβ, with four of these mutations located within the $Aβ_{18-22}$ sequence (Figure 4). The same four amino acid mutations in $Aβ_{18-22}$ (including A21G) inhibit Aβ hydrolysis by NEP.[70] Proteolysis within this targeted region has been shown to reduce Aβ aggregation and neurotoxicity.[73−75] Increasing NEP specificity for $Aβ_{18-22}$ is likely to retain the therapeutic potential of the peptidase while mitigating side effects from promiscuous off-target peptide degradation. Our models could guide mutations to the NEP S2′ site that increase specificity for $Aβ_{18-22}$ by decreasing the affinity for non-Aβ substrates. One potential target for mutation is the S2′ residue F106, whose side-chain does not appear to contribute to the binding of Aβ in our model. We predict that an F106W mutation will significantly reduce the volume of the S2′ subsite of NEP, having little effect on the binding of Aβ but potentially reducing affinity for ligands with large or bulky P2′ groups, such as Phosphoramidon, CGS30008, and [Ala^2,Met^5]-enkephalin.[72]

CONCLUSION

X-ray crystallography, site-directed mutagenesis, and in vitro/in vivo studies have provided critical insights about NEP structure and activity, including degradation of Aβ peptides. Using these studies as validation, we have modeled the binding interactions and ΔG° of NEP with inhibitors and sequences of Aβ. The models of NEP show novel binding interactions between bound sequences of Aβ and the R102/R110 side-chains of the NEP S2′ subsite, suggesting that S2′ site residues may form interactions specific to the binding of certain NEP substrates. Site-directed mutagenesis of the S2′ residues can be used to confirm or refine the proposed NEP−Aβ model, which in turn may guide NEP mutations that alter the binding specificity in favor of Aβ. Derivatives of NEP with increased specificity for Aβ have greater potential to safely and selectively reduce the accumulation of Aβ observed with the progression of AD. To this end, our model of Aβ in NEP is a useful starting point for developing the therapeutic potential of NEP-mediated degradation of Aβ.

ASSOCIATED CONTENT

Supporting Information

Figures S1−S9 representing analyses of data obtained from the docking of each NEP inhibitor and sequence of Aβ. Plots of ligand RMSD (Figures S1−S4 and S7−S9) depicting the averaged distance of all ligand atoms from an initial docked pose during a simulation and representing evidence for the stability of ligand docking interactions with NEP. This material is available free of charge via the Internet at http://pubs.acs.org.

AUTHOR INFORMATION

Corresponding Author

*Phone: 412-396-1894. E-mail: casciom@duq.edu.

Notes

The authors declare no competing financial interest.

ACKNOWLEDGMENTS

We are grateful to Scott Boesch for his technical assistance and Dr. Marc Glucksman for helpful discussions. We also acknowledge support provided by a CURE grant from the Pennsylvania Department of Health.

ABBREVIATIONS

Aβ, amyloid beta or beta-amyloid peptide; AD, Alzheimer's disease; ΔG°, change in Gibb's free energy upon binding under standard conditions; $ΔG°_{EXP}$, $ΔG°_{GBVI}$, or $ΔG°_{PBSA}$, experimental ΔG°, or GBVI or PBSA scoring estimates of ΔG°, respectively; GBVI, generalized Born volume integral; PBSA, Poisson−Boltzmann plus surface area; MD, molecular dynamics; MOE, Molecular Operating Environment; NEP, Neprilysin; *R*, Pearson's correlation coefficient; RMS, root-mean-square

REFERENCES

(1) Turner, A. J.; Isaac, R. E.; Coates, D. The Neprilysin (NEP) Family of Zinc Metalloendopeptidases: Genomics and Function. *Bioessays* **2001**, *23*, 261−269.

(2) Turner, A. J.; Tanzawa, K. Mammalian Membrane Metallopeptidases: NEP, ECE, KELL, and PEX. *FASEB J.* **1997**, *11*, 355−364.

(3) Roques, B. P.; Noble, F.; Dauge, V.; Fournie-Zaluski, M. C.; Beaumont, A. Neutral Endopeptidase 24.11: Structure, Inhibition, and Experimental and Clinical Pharmacology. *Pharmacol. Rev.* **1993**, *45*, 87−146.

(4) Miners, J. S.; van Helmond, Z.; Kehoe, P. G.; Love, S. Changes with Age in the Activities of Beta-Secretase and the a Beta-Degrading Enzymes Neprilysin, Insulin-Degrading Enzyme and Angiotensin-Converting Enzyme. *Brain Pathol.* **2010**, *20*, 794−802.

(5) Wang, S. Q.; Wang, R.; Chen, L.; Bennett, D. A.; Dickson, D. W.; Wang, D. S. Expression and Functional Profiling of Neprilysin, Insulin-Degrading Enzyme, and Endothelin-Converting Enzyme in Prospectively Studied Elderly and Alzheimer's Brain. *J. Neurochem.* **2010**, *115*, 47−57.

(6) Nalivaeva, N. N.; Fisk, L. R.; Belyaev, N. D.; Turner, A. J. Amyloid-Degrading Enzymes as Therapeutic Targets in Alzheimer's Disease. *Curr. Alzheimer. Res.* **2008**, *5*, 212−224.

(7) Hardy, J.; Selkoe, D. J. Medicine - the Amyloid Hypothesis of Alzheimer's Disease: Progress and Problems on the Road to Therapeutics. *Science* **2002**, *297*, 353−356.

(8) Mawuenyega, K. G.; Sigurdson, W.; Ovod, V.; Munsell, L.; Kasten, T.; Morris, J. C.; Yarasheski, K. E.; Bateman, R. J. Decreased Clearance of CNS Beta-Amyloid in Alzheimer's Disease. *Science* **2010**, *330*, 1774.

(9) Miners, J. S.; Barua, N.; Kehoe, P. G.; Gill, S.; Love, S. Abeta-Degrading Enzymes: Potential for Treatment of Alzheimer Disease. *J. Neuropathol. Exp. Neurol.* **2011**, *70*, 944−959.

(10) Ahmed, M.; Davis, J.; Aucoin, D.; Sato, T.; Ahuja, S.; Aimoto, S.; Elliott, J. I.; Van Nostrand, W. E.; Smith, S. O. Structural Conversion of Neurotoxic Amyloid-Beta(1−42) Oligomers to Fibrils. *Nat. Struct. Mol. Bio.* **2010**, *17*, 561−567.
(11) Goedert, M.; Spillantini, M. G. A Century of Alzheimer's Disease. *Science* **2006**, *314*, 777−781.
(12) Dahlgren, K. N.; Manelli, A. M.; Stine, W. B., Jr.; Baker, L. K.; Krafft, G. A.; LaDu, M. J. Oligomeric and Fibrillar Species of Amyloid-Beta Peptides Differentially Affect Neuronal Viability. *J. Biol. Chem.* **2002**, *277*, 32046−32053.
(13) Maezawa, I.; Zimin, P.; Wulff, H.; Jin, L.-W. Amyloid-Beta Protein Oligomer at Low Nanomolar Concentrations Activates Microglia and Induces Microglial Neurotoxicity. *J. Biol. Chem.* **2011**, *286*, 3693−3706.
(14) Ono, K.; Condron, M. M.; Teplow, D. B. Structure-Neurotoxicity Relationships of Amyloid Beta-Protein Oligomers. *Proc. Natl. Acad. Sci. U.S.A.* **2009**, *106*, 14745−14750.
(15) Hartley, D. M.; Walsh, D. M.; Ye, C. P.; Diehl, T.; Vasquez, S.; Vassilev, P. M.; Teplow, D. B.; Selkoe, D. J. Protofibrillar Intermediates of Amyloid Beta-Protein Induce Acute Electrophysiological Changes and Progressive Neurotoxicity in Cortical Neurons. *J. Neurosci.* **1999**, *19*, 8876−8884.
(16) Zhang, Y.; McLaughlin, R.; Goodyer, C.; LeBlanc, A. Selective Cytotoxicity of Intracellular Amyloid Beta Peptide1−42 through P53 and Bax in Cultured Primary Human Neurons. *J. Cell. Biol.* **2002**, *156*, 519−529.
(17) Citron, M. Alzheimer's Disease: Strategies for Disease Modification. *Nat. Rev. Drug Discovery* **2010**, *9*, 387−398.
(18) Weiner, H. L.; Frenkel, D. Immunology and Immunotherapy of Alzheimer's Disease. *Nat. Rev. Immunol.* **2006**, *6*, 490.
(19) De Strooper, B. Proteases and Proteolysis in Alzheimer Disease: A Multifactorial View on the Disease Process. *Physiol. Rev.* **2010**, *90*, 465−494.
(20) Hamley, I. W. The Amyloid Beta Peptide: A Chemist's Perspective. Role in Alzheimer's and Fibrillization. *Chem. Rev.* **2012**, 5147−5192.
(21) Serpell, L. C.; Blake, C. C.; Fraser, P. E. Molecular Structure of a Fibrillar Alzheimer's A beta Fragment. *Biochemistry* **2000**, *39*, 13269−13275.
(22) Selkoe, D. J.; Schenk, D. Alzheimer's Disease: Molecular Understanding Predicts Amyloid-Based Therapeutics. *Annu. Rev. Pharmacol. Toxicol.* **2003**, *43*, 545−584.
(23) Teplow, D. B. Structural and Kinetic Features of Amyloid Beta-Protein Fibrillogenesis. *Amyloid* **1998**, *5*, 121−142.
(24) Shirotani, K.; Tsubuki, S.; Iwata, N.; Takaki, Y.; Harigaya, W.; Maruyama, K.; Kiryu-Seo, S.; Kiyama, H.; Iwata, H.; Tomita, T.; Iwatsubo, T.; Saido, T. C. Neprilysin Degrades Both Amyloid Beta Peptides 1−40 and 1−42 Most Rapidly and Efficiently among Thiorphan- and Phosphoramidon-Sensitive Endopeptidases. *J. Biol. Chem.* **2001**, *276*, 21895−21901.
(25) Miners, J. S.; Baig, S.; Palmer, J.; Palmer, L. E.; Kehoe, P. G.; Love, S. A Beta-Degrading Enzymes in Alzheimer's Disease. *Brain Pathol.* **2008**, *18*, 240−252.
(26) Iwata, N.; Tsubuki, S.; Takaki, Y.; Shirotani, K.; Lu, B.; Gerard, N. P.; Gerard, C.; Hama, E.; Lee, H. J.; Saido, T. C. Metabolic Regulation of Brain a Beta by Neprilysin. *Science* **2001**, *292*, 1550−1552.
(27) Iwata, N.; Tsubuki, S.; Takaki, Y.; Watanabe, K.; Sekiguchi, M.; Hosoki, E.; Kawashima-Morishima, M.; Lee, H. J.; Hama, E.; Sekine-Aizawa, Y.; Saido, T. C. Identification of the Major Abeta(1−42)-Degrading Catabolic Pathway in Brain Parenchyma: Suppression Leads to Biochemical and Pathological Deposition. *Nat. Med.* **2000**, *6*, 143−150.
(28) Iwata, N.; Mizukami, H.; Shirotani, K.; Takaki, Y.; Muramatsu, S.; Lu, B.; Gerard, N. P.; Gerard, C.; Ozawa, K.; Saido, T. C. Presynaptic Localization of Neprilysin Contributes to Efficient Clearance of Amyloid-Beta Peptide in Mouse Brain. *J. Neurosci.* **2004**, *24*, 991−998.
(29) El-Amouri, S. S.; Zhu, H.; Yu, J.; Marr, R.; Verma, I. M.; Kindy, M. S. Neprilysin: An Enzyme Candidate to Slow the Progression of Alzheimer's Disease. *Am. J. Pathol.* **2008**, *172*, 1342−1354.
(30) Tampellini, D.; Rahman, N.; Lin, M. T.; Capetillo-Zarate, E.; Gouras, G. K. Impaired Beta-Amyloid Secretion in Alzheimer's Disease Pathogenesis. *J. Neurosci.* **2011**, *31*, 15384−15390.
(31) Marr, R. A.; Guan, H.; Rockenstein, E.; Kindy, M.; Gage, F. H.; Verma, I.; Masliah, E.; Hersh, L. B. Neprilysin Regulates Amyloid Beta Peptide Levels. *J. Mol. Neurosci.* **2004**, *22*, 5−11.
(32) Hemming, M. L.; Patterson, M.; Reske-Nielsen, C.; Lin, L.; Isacson, O.; Selkoe, D. J. Reducing Amyloid Plaque Burden Via Ex Vivo Gene Delivery of an a Beta-Degrading Protease: A Novel Therapeutic Approach to Alzheimer Disease. *PLoS Med.* **2007**, *4*, 1405−1416.
(33) Li, Y.; Wang, J.; Liu, J.; Liu, F. A Novel System for in Vivo Neprilysin Gene Delivery Using a Syringe Electrode. *J. Neurosci. Methods* **2010**, *193*, 226−231.
(34) Guan, H.; Liu, Y.; Daily, A.; Police, S.; Kim, M.-H.; Oddo, S.; LaFerla, F. M.; Pauly, J. R.; Murphy, M. P.; Hersh, L. B. Peripherally Expressed Neprilysin Reduces Brain Amyloid Burden: A Novel Approach for Treating Alzheimer's Disease. *J. Neurosci. Res.* **2009**, *87*, 1462−1473.
(35) Liu, Y.; Studzinski, C.; Beckett, T.; Guan, H.; Hersh, M. A.; Murphy, M. P.; Klein, R.; Hersh, L. B. Expression of Neprilysin in Skeletal Muscle Reduces Amyloid Burden in a Transgenic Mouse Model of Alzheimer Disease. *Mol. Ther.* **2009**, *17*, 1381−1386.
(36) Liu, Y.; Studzinski, C.; Beckett, T.; Murphy, M. P.; Klein, R. L.; Hersh, L. B. Circulating Neprilysin Clears Brain Amyloid. *Mol. Cell. Neurosci.* **2010**, *45*, 101−107.
(37) Spencer, B.; Marr, R. A.; Gindi, R.; Potkar, R.; Michael, S.; Adame, A.; Rockenstein, E.; Verma, I. M.; Masliah, E. Peripheral Delivery of a CNS Targeted, Metalo-Protease Reduces Ab Toxicity in a Mouse Model of Alzheimer's Disease. *PLoS One* **2011**, *6*, 1−12.
(38) Iijima-Ando, K.; Hearn, S. A.; Granger, L.; Shenton, C.; Gatt, A.; Chiang, H. C.; Hakker, I.; Zhong, Y.; Iijima, K. Overexpression of Neprilysin Reduces Alzheimer Amyloid-Beta 42 (Abeta 42)-Induced Neuron Loss and Intraneuronal Abeta 42 Deposits but Causes a Reduction in Camp-Responsive Element-Binding Protein-Mediated Transcription, Age-Dependent Axon Pathology, and Premature Death in Drosophila. *J. Biol. Chem.* **2008**, *283*, 19066−19076.
(39) Aharoni, A.; Gaidukov, L.; Khersonsky, O.; Gould, S. M.; Roodveldt, C.; Tawfik, D. S. The 'Evolvability' of Promiscuous Protein Functions. *Nat. Genet.* **2005**, *37*, 73−76.
(40) Sexton, T.; Hitchcook, L. J.; Rodgers, D. W.; Bradley, L. H.; Hersh, L. B. Active Site Mutations Change the Cleavage Specificity of Neprilysin. *PLoS One* **2012**, *7*, e32343.
(41) Oefner, C.; Roques, B. P.; Fournie-Zaluski, M. C.; Dale, G. E. Structural Analysis of Neprilysin with Various Specific and Potent Inhibitors. *Acta Crystallogr., Sect. D: Biol. Crystallogr.* **2004**, *60*, 392−396.
(42) Oefner, C.; D'Arcy, A.; Hennig, M.; Winkler, F. K.; Dale, G. E. Structure of Human Neutral Endopeptidase (Neprilysin) Complexed with Phosphoramidon. *J. Mol. Biol.* **2000**, *296*, 341−349.
(43) Oefner, C.; Pierau, S.; Schulz, H.; Dale, G. E. Structural Studies of a Bifunctional Inhibitor of Neprilysin and Dpp-Iv. *Acta Crystallogr. Sect. D: Biol. Crystallogr.* **2007**, *63*, 975−981.
(44) Dale, G. E.; Oefner, C. Neprilysin. In *Handbook of Metalloproteins*; John Wiley & Sons, Ltd.: Chichester, West-Sussex, United Kingdom, 2006; pp 1−12.
(45) Glossop, M. S.; Bazin, R. J.; Dack, K. N.; Fox, D. N.; MacDonald, G. A.; Mills, M.; Owen, D. R.; Phillips, C.; Reeves, K. A.; Ringer, T. J.; Strang, R. S.; Watson, C. A. Synthesis and Evaluation of Heteroarylalanine Diacids as Potent and Selective Neutral Endopeptidase Inhibitors. *Bioorg. Med. Chem. Lett.* **2011**, *21*, 3404−3406.
(46) Sahli, S.; Frank, B.; Schweizer, W. B.; Diederich, F.; Blum-Kaelin, D.; Aebi, J. D.; Böhm, H.-J.; Oefner, C.; Dale, G. E. Second-Generation Inhibitors for the Metalloprotease Neprilysin Based on Bicyclic Heteroaromatic Scaffolds: Synthesis, Biological Activity, and X-Ray Crystal-Structure Analysis. *Helv. Chim. Acta* **2005**, *88*, 731−750.

(47) Gomez-Monterrey, I.; Turcaud, S.; Lucas, E.; Bruetschy, L.; Roques, B. P.; Fournie-Zaluski, M. C. Exploration of Neutral Endopeptidase Active Site by a Series of New Thiol-Containing Inhibitors. *J. Med. Chem.* **1993**, *36*, 87−94.
(48) Schechter, I.; Berger, A. On the Size of the Active Site in Proteases. I. Papain. *Biochem. Biophys. Res. Commun.* **1967**, *27*, 157−162.
(49) Pope, D.; Cascio, M. Neprilysin Inhibitors Provide Insight into Its Specificity and Therapeutic Potential. In *Frontiers in Drug Design & Discovery*, 6 ed.; Atta-ur-Rahman, Choudhary, M. I., Eds.; Bentham Science Publishers: Sharjah, United Arab Emirates, 2014; Vol. *6*, pp 353−377.
(50) Manzetti, S. Computer Modeling and Nanosecond Simulation of the Enzyme-Substrate Complex of the Common Lymphoblastic Leukemia Antigen (Neprilysin) Indicates Shared Residues at the Primary Specificity Pocket (S1′) with Matrix Metalloproteases. *J. Mol. Model.* **2003**, *9*, 348−354.
(51) Dimitropoulos, N.; Papakyriakou, A.; Dalkas, G. A.; Sturrock, E. D.; Spyroulias, G. A. A Computational Approach to the Study of the Binding Mode of Dual ACE/NEP Inhibitors. *J. Chem. Inf. Model.* **2010**, *50*, 388−396.
(52) *Molecular Operating Environment (MOE)*, 2011.10; Chemical Computing Group, Inc.: Montreal, QC, Canada, 2011.
(53) Corbeil, C. R.; Williams, C. I.; Labute, P. Variability in Docking Success Rates Due to Dataset Preparation. *J. Comput.-Aided Mol. Des.* **2012**, *26*, 775−786.
(54) Mikulskis, P.; Genheden, S.; Rydberg, P.; Sandberg, L.; Olsen, L.; Ryde, U. Binding Affinities in the Sampl3 Trypsin and Host-Guest Blind Tests Estimated with the Mm/Pbsa and Lie Methods. *J. Comput.-Aided Mol. Des.* **2012**, *26*, 527−541.
(55) Kollman, P. A.; Massova, I.; Reyes, C.; Kuhn, B.; Huo, S.; Chong, L.; Lee, M.; Lee, T.; Duan, Y.; Wang, W.; Donini, O.; Cieplak, P.; Srinivasan, J.; Case, D. A.; Cheatham, T. E., 3rd. Calculating Structures and Free Energies of Complex Molecules: Combining Molecular Mechanics and Continuum Models. *Acc. Chem. Res.* **2000**, *33*, 889−897.
(56) Crescenzi, O.; Tomaselli, S.; Guerrini, R.; Salvadori, S.; D'Ursi, A. M.; Temussi, P. A.; Picone, D. Solution Structure of the Alzheimer Amyloid Beta-Peptide (1−42) in an Apolar Microenvironment. Similarity with a Virus Fusion Domain. *Eur. J. Biochem.* **2002**, *269*, 5642−5648.
(57) Bayly, C.; Mckay, D.; Truchon, J.-F. An Informal Amber Small Molecule Force Field: Parm@Frosst, 2010. CCL.net. http://www.ccl.net/cca/data/parm_at_Frosst/ (accessed April 12, 2012).
(58) Jakalian, A.; Jack, D. B.; Bayly, C. I. Fast, Efficient Generation of High-Quality Atomic Charges. AM1-BCC Model: II. Parameterization and Validation. *J. Comput. Chem.* **2002**, *23*, 1623−1641.
(59) Chen, H.; Noble, F.; Mothe, A.; Meudal, H.; Coric, P.; Danascimento, S.; Roques, B. P.; George, P.; Fournie-Zaluski, M. C. Phosphinic Derivatives as New Dual Enkephalin-Degrading Enzyme Inhibitors: Synthesis, Biological Properties, and Antinociceptive Activities. *J. Med. Chem.* **2000**, *43*, 1398−1408.
(60) Marie-Claire, C.; Ruffet, E.; Antonczak, S.; Beaumont, A.; O'Donohue, M.; Roques, B. P.; Fournie-Zaluski, M. C. Evidence by Site-Directed Mutagenesis that Arginine 203 of Thermolysin and Arginine 717 of Neprilysin (Neutral Endopeptidase) Play Equivalent Critical Roles in Substrate Hydrolysis and Inhibitor Binding. *Biochemistry* **1997**, *36*, 13938−13945.
(61) Fournie-Zaluski, M. C.; Gonzalez, W.; Turcaud, S.; Pham, I.; Roques, B. P.; Michel, J. B. Dual Inhibition of Angiotensin-Converting Enzyme and Neutral Endopeptidase by the Orally Active Inhibitor Mixanpril: A Potential Therapeutic Approach in Hypertension. *Proc. Natl. Acad. Sci. U.S.A.* **1994**, *91*, 4072−4076.
(62) Fournie-Zaluski, M. C.; Lucas, E.; Waksman, G.; Roques, B. P. Differences in the Structural Requirements for Selective Interaction with Neutral Metalloendopeptidase (Enkephalinase) or Angiotensin-Converting Enzyme. Molecular Investigation by Use of New Thiol Inhibitors. *Eur. J. Biochem.* **1984**, *139*, 267−274.
(63) Fink, C. A.; Qiao, Y.; Berry, C. J.; Sakane, Y.; Ghai, R. D.; Trapani, A. J. New Alpha-Thiol Dipeptide Dual Inhibitors of Angiotensin-I Converting Enzyme and Neutral Endopeptidase EC 3.4.24.11. *J. Med. Chem.* **1995**, *38*, 5023−5030.
(64) Roderick, S. L.; Fournie-Zaluski, M. C.; Roques, B. P.; Matthews, B. W. Thiorphan and Retro-Thiorphan Display Equivalent Interactions When Bound to Crystalline Thermolysin. *Biochemistry* **1989**, *28*, 1493−1497.
(65) Dion, N.; Le Moual, H.; Fournie-Zaluski, M. C.; Roques, B. P.; Crine, P.; Boileau, G. Evidence That Asn542 of Neprilysin (EC 3.4.24.11) is Involved in Binding of the P2′ Residue of Substrates and Inhibitors. *Biochem. J.* **1995**, *311*, 623−627.
(66) Tiraboschi, G.; Jullian, N.; Thery, V.; Antonczak, S.; Fournie-Zaluski, M. C.; Roques, B. P. A Three-Dimensional Construction of the Active Site (Region 507−749) of Human Neutral Endopeptidase (EC.3.4.24.11). *Protein Eng.* **1999**, *12*, 141−149.
(67) Leissring, M. A.; Lu, A.; Condron, M. M.; Teplow, D. B.; Stein, R. L.; Farris, W.; Selkoe, D. J. Kinetics of Amyloid Beta-Protein Degradation Determined by Novel Fluorescence- and Fluorescence Polarization-Based Assays. *J. Biol. Chem.* **2003**, *278*, 37314−37320.
(68) Howell, S.; Nalbantoglu, J.; Crine, P. Neutral Endopeptidase Can Hydrolyze Beta-Amyloid(1−40) but Shows No Effect on Beta-Amyloid Precursor Protein Metabolism. *Peptides* **1995**, *16*, 647−652.
(69) Tsubuki, S.; Takaki, Y.; Saido, T. C. Dutch, Flemish, Italian, and Arctic Mutations of APP and Resistance of Abeta to Physiologically Relevant Proteolytic Degradation. *Lancet* **2003**, *361*, 1957−1958.
(70) Betts, V.; Leissring, M. A.; Dolios, G.; Wang, R.; Selkoe, D. J.; Walsh, D. M. Aggregation and Catabolism of Disease-Associated Intra-Abeta Mutations: Reduced Proteolysis of Abeta(A21G) by Neprilysin. *Neurobiol. Dis.* **2008**, *31*, 442−450.
(71) Hersh, L. B.; Rodgers, D. W. Neprilysin and Amyloid Beta Peptide Degradation. *Curr. Alzheimer Res.* **2008**, *5*, 225−231.
(72) Kim, Y. A.; Shriver, B.; Quay, T.; Hersh, L. B. Analysis of the Importance of Arginine 102 in Neutral Endopeptidase (Enkephalinase) Catalysis. *J. Biol. Chem.* **1992**, *267*, 12330−12335.
(73) Liao, M. Q.; Tzeng, Y. J.; Chang, L. Y.; Huang, H. B.; Lin, T. H.; Chyan, C. L.; Chen, Y. C. The Correlation between Neurotoxicity, Aggregative Ability and Secondary Structure Studied by Sequence Truncated Abeta Peptides. *FEBS Lett.* **2007**, *581*, 1161−1165.
(74) Liu, R.; McAllister, C.; Lyubchenko, Y.; Sierks, M. R. Residues 17−20 and 30−35 of Beta-Amyloid Play Critical Roles in Aggregation. *J. Neurosci. Res.* **2004**, *75*, 162−171.
(75) Mukherjee, A.; Song, E.; Kihiko-Ehmann, M.; Goodman, J. P., Jr.; Pyrek, J. S.; Estus, S.; Hersh, L. B. Insulysin Hydrolyzes Amyloid Beta Peptides to Products that are Neither Neurotoxic nor Deposit on Amyloid Plaques. *J. Neurosci.* **2000**, *20*, 8745−8749.